Interlayer surface relaxations and energies of fcc metal surfaces by a tight-binding method

Michael I. Haftel, Noam Bernstein, Michael J. Mehl, and Dimitris A. Papaconstantopoulos
Center for Computational Materials Science, Naval Research Laboratory, Washington, DC 20375-5343, USA
(Received 13 August 2003; revised manuscript received 10 March 2004; published 22 September 2004)

The authors examine the interlayer surface relaxations and surface energies for the low-index faces of fcc Ni, Pd, Rh, Pt, Au, and Ir using the Naval Research Laboratory (NRL) tight-binding (TB) method. We compare the TB calculations, utilizing self-consistent charge transfer, with experimental measurements, density functional theory (DFT) calculations, and semiempirical methods. We find that for these metals the NRL-TB method largely reproduces the trends with respect to the exposed face and periodic table position obtained in DFT calculations and experimental measurements. We find that the inclusion of self-consistency in the TB surface calculations is essential for obtaining this agreement, as the TB calculations without it predict large first interlayer expansions for many of these surfaces. We also examine the energetics and relaxations of the 2×1 (011) missing row reconstruction for these metals. The TB method predicts that, in agreement with experiment, Au and Pt undergo this reconstruction, while Ni, Pd, and Rh do not, but predicts the Ir ground state structure to be unreconstructed 1×1, opposite to experiment. The interatomic relaxations of the (011) missing row structure for Pt, Au, and Ir are in good agreement with DFT calculations and experiment. Finally, we analyze the bonding characteristics of these metals using a decomposition of the TB total energy over neighboring atoms and angular momentum character.

DOI: 10.1103/PhysRevB.70.125419 PACS number(s): 68.47.De, 68.35.Bs, 68.35.Md

I. INTRODUCTION

The tight-binding (TB) method[1–3] is becoming a reliable method to accurately describe the structure, dynamics, and electronic structure for systems of hundreds of atoms that are impractical for first-principles methods. In particular, investigation of surface phenomena such as diffusion, the role of defects, islanding and growth can be calculated efficiently using TB methods. While semiempirical methods such as the embedded-atom method[4] (EAM) have met with some success in this regard for metals, or more generally the modified embedded atom method[5] (MEAM) or bond-order type potentials for metals and semiconductors,[6,7] anomalies often appear once one gets away from the atomic environment to which these potentials are fit. Furthermore, these methods cannot calculate electronic properties at all, thus questions concerning the surface density of states, the effects of surface states, or surface magnetism cannot be addressed by these semiempirical methods. The TB formalism retains a form closely resembling the underlying density functional theory (DFT) underpinnings, including, e.g., angular forces that are often introduced in an *ad hoc* manner in other semiempirical methods. Thus the TB method should be more extendable to environments differing from those to which it was fit, i.e., it should be highly transferable.

NRL has embarked on a program to develop highly transferable TB parametrizations throughout the periodic table. Details of this program have appeared previously.[2,3,8] Most of these parametrizations have been carried out for single metal systems, but many have also been developed for alloys[9] and semiconductors[10,11] including binary systems. By fitting the first-principles full potential linearized or muffin-tin augmented plane wave (APW)[12] DFT equations of state and band structures for fcc and bcc metals, the NRL-TB parametrizations typically yield structural energies, elastic constants, vacancy formation energies, and strain properties in good agreement with experiment or DFT calculations even when the ground state is not bcc or fcc. This indicates high transferability. A molecular dynamics program has also been developed at NRL utilizing this TB method.[13]

This paper evaluates the NRL-TB method for metals in the surface environment. The NRL-TB method has not been extensively tested at surfaces. The surface presents a challenge for any method because, first, the atomic coordination is much lower than in the bulk, and second, the atomic environment is very asymmetric, i.e., one sided. This makes the surface very different from the bulk environment to which these methods are typically fit. Some empirical methods, such as the surface embedded atom method (SEAM)[14] and some MEAM models[15] have employed surface properties as part of the fitting database. To date this has not been the case for the NRL-TB method. Our hope is that the underlying physics of the method would yield applicability far beyond its original fitting database.

We examine the surface energies, interlayer separations, and (011) missing row reconstructions calculated by the NRL-TB method for the fcc metals Ni, Pd, Rh, Ir, Pt, and Au. While there exist a number of TB calculations examining electronic and magnetic structure,[16–20] atomic structure,[21–26] and diffusion[27] for metal surfaces and clusters,[21,28–30] to our knowledge there exist no consistent surveys of the TB approximation for metal surfaces. Surface phenomena represent a potentially extremely rich area for the TB method, with possible application to surface magnetism, the role of strain, and the formation and properties of self-assembled quantum dots. This present work is a first step in the direction of applying the NRL-TB method to these more complex problems. Many of these represent environments even more asymmetric and under-coordinated than those in the present study. Somewhere (e.g., small clusters) conditions may be such that our TB method might break down. In this paper we restrict ourselves to judging the current

NRL-TB method with certain surface phenomena. This will give us a good idea on its transferability to less coordinated structures. At some point tailoring the parameters to surfaces and low coordination structures may become necessary to reliably predict certain surface phenomena (small clusters, structure of monolayers, etc.).

We regard the present study as a prelude to more complex problems. However, surface relaxation and reconstructions have generated considerable interest in their own right. Extensive experimental investigations with low energy electron diffraction (LEED),[31–40] low and medium energy ion scattering (LEIS, MEIS),[41,42] and by other techniques[43,44]on these metals have been taking place for over two decades. They have also been extensively examined with the EAM,[45–47] related methods,[14,48] and the MEAM,[15,49–51] providing testing grounds for these methods. Some DFT[52–61] and related[62] calculations exist as well. Where possible, we compare to DFT and experimental results. Despite extensive investigation, some phenomena still lack satisfactory explanation. The experimentally observed first interlayer expansion of Rh(001) (Ref. 35) and Pd(001) (Ref. 37) is not predicted by DFT[53,54] or any present semiempirical method.[15,47,48] The role of stress in accounting for the surface reconstructions of Au is not yet clearly resolved.[63] Also, the detailed structure of the Ir(011) reconstruction is not clear.[41] The TB method may provide insight into these anomalies.

In Sec. II of this paper we briefly review the NRL-TB method.[2,3,8] We describe our calculation of the surface relaxation and reconstructions using the NRL-TB code modified for charge self-consistency.[11,64] The non-self-consistent NRL-TB method is about three orders of magnitude faster than APW methods.[8] The self-consistent TB (SCTB) method typically requires about 10 self-consistency iterations for convergence in surface calculations, making it about two orders of magnitude faster than APW methods. While it is difficult to compare SCTB with EAM timings because of different scaling with number of atoms and cell size, some preliminary comparisons indicate that the EAM would be 4–6 orders of magnitude faster than SCTB for problems with $\sim$100 atoms, but without electronic structure information. In Sec. III we present the TB predictions for the interlayer separations (including the role of self-consistency), surface energies and (011) missing row reconstructions for Ni, Pd, Rh, Ir, Pt, and Au. We compare our results to experiment, DFT, EAM, and MEAM calculations. In our comparisons with the EAM and MEAM we include typical results. Many versions of these and related models exist[67–69] and surface results can vary substantially from model to model. Likewise, many different types of DFT calculations exist (e.g., those using GGA versus LDA, those using all electron methods versus pseudopotential methods, etc.) with varying results. Again, the comparisons made are not exhaustive. We briefly indicate in our tables the type of DFT calculation with which comparisons are made.

Although we have extended our TB method to handle ferromagnetism[65] and developed TB parameters for ferromagnetic Ni, we consider paramagnetic Ni since at present our TB code can only handle paramagnetic Ni self-consistently. Additionally, EAM[47] and MEAM[49] calculations with which to compare are available only for the paramagnetic state. Pd, Rh, Pt, and Ir are of interest as catalytic surfaces. Rh exhibits possible surface ferromagnetism.[29,30,66] Rh and Pd (001) have anomalous interlayer expansion at the surface.[35,37] Pt, Au, and Ir, unique among transition metals, exhibit surface reconstructions on low-index faces.[41,42,44]

We find that generally the TB method gives good agreement with experiment and DFT calculations. The agreement is typically somewhat better than that of the EAM or MEAM with regards to individual surface relaxation quantities. However, the TB method performs significantly better for predicting the variations in the surface energies and interlayer spacings as one proceeds across the periodic table or between different surfaces of the same metal. In Sec. IV we discuss the reasons for success of the TB method for these surfaces. We calculate the nearest-neighbor in-plane and out-of-plane bond strengths as predicted by the TB method for a number of metals in the 4*d* and 5*d* shells, and examine the trends in the *s*-*p*-*d* bonding across these shells in the bulk and at the surface. The TB method here generally reproduces the transition from a bonding to antibonding role for *d*-states across these shells, thus conforming to the correct quantum mechanical behavior. The repression of this *d*-state antibonding at the surface through increased s*p* attraction indicated by our TB analyses is a likely mechanism for the surface reconstruction of the late 5*d* metals. Section V gives our concluding remarks. The main conclusion is that the TB method gives a good description of the surfaces of these fcc metals and thus is transferable to the surface environment.

II. THE NRL TIGHT BINDING METHOD

We stress here that the NRL-TB method uses a nonorthogonal TB Hamiltonian, which turns out to be crucial for determining surface energies. Both the hopping and on-site parameters are bondlength and environment dependent, and the method is formulated in such a way so that the repulsive potential used in the so-called "glue" methods is not required.

Details of the NRL-TB method are described elsewhere.[2,3,8] Parametrizations are available for over 35 elements including most metals. The parameters are fit to the APW band structure and equation of state for fcc and bcc structures, and give results in good agreement with APW predictions for most other bulk properties.[3,8] Programs for fitting the TB parameters, static total energy calculations, and molecular dynamics (MD) are available through the Common HPC Software Support Initiative (CHSSI) of the Department of Defense. Details on the use of the TB parameters and programs are available on the NRL-TB web site http://cst-www.nrl.navy.mil/bind/. In its original form, the NRL-TB method has been tested in many ways including elastic constants, vacancy formation and stacking fault energies, ductility and thermal expansion, with generally good agreement with experiment.[3,8] Similar results are also seen for binary compounds[8,70,71] and semiconductors. In this work we use the 16.5 a.u. cutoff for Pd, the paramagnetic parameterization for Ni, and the "99" version for Au used in Ref. 13 (which was fit to simple cubic as well as to fcc and bcc structures). All the other parameterizations are those described in Ref. 3.

To precisely understand particular surface phenomena, especially low coordinated systems such as clusters and monolayers, it is often useful to fit TB parameters to small clusters and surfaces. This procedure has been successful in particular in TB studies of H_2 dynamics on Pd surfaces[71] and of surface magnetism of Co monolayers and clusters.[72]Our concentration, however, is on the assessment of our present TB method for a range of surface phenomena for single crystal fcc metals, with an eye toward more extended application to metal surfaces. This study should indicate to what degree it may become necessary to expand our database to fitting surfaces.

We carry out the calculation of the surface energies and surface relaxations utilizing the TB code modified for self-consistency. For the unreconstructed 1×1 structures we employ a unit cell consisting of 24 atomic layers and 13 vacant layers (between slabs) for (111) surfaces, seven vacant layers for (001) surfaces, and nine vacant layers for (011) surfaces. We employ meshes of 200 special *k*-points ($20\times20\times1$) for (001), 192 ($16\times24\times1$) for (011), and 192 ($24\times16\times1$) for (111). (The ratios of indices are roughly in proportion to the lengths of the reciprocal lattice vectors.) All atoms are completely relaxed using the conjugate gradient method, and charge transfer is taken into account self-consistently.[11,64] In calculating the bulk energy per atom to be used in the surface energy calculation for each face, we employ the same supercell as the surface calculation, with the same *k*-points, except that the vacuum layers are filled.

To examine the (011) 2×1 missing-row reconstruction we employ a 16-layer 2×1 cell. We first carry out a bulk calculation consisting of the above unit cell with no vacuum layers. We use 432 *k* points ($12\times36\times2$) for this calculation. We simulate the unreconstructed 1×1 surface using a modification of the bulk unit cell with 16 additional vacuum layers and with 216 *k* points ($12\times36\times1$) to get consistent results to compare with the previous bulk calculation and accurately determine the unreconstructed 1×1 surface energy. Finally we repeat the latter calculation, but with one additional atom on the seventeenth layer to simulate the 2×1 missing row reconstruction. In this way we can get a very accurate determination of the surface energy difference between the reconstructed and unreconstructed phases.

III. RESULTS

A. Surface energies and relaxation for 1X1 surfaces

Tables I–VI contain the main results for the TB predictions of the surface energies and interlayer separations for the low-index faces of the fcc metals considered. These tables give the first three interlayer separations ($\Delta d_{12}, \Delta d_{23}, \Delta d_{34}$) and the surface energy (γ) for the (001), (011), and (111) faces of Ni, Rh, Pd, Ir, Pt, and Au, respectively. Experimental results and results of DFT, EAM (including related methods), and MEAM calculations are also shown, where available. Tables II and III also give surface energies as predicted by other TB methods.[21,28] Face-specific experimental surface energies are not generally available; the experimental points in the tables represent measurements on polycrystalline samples,[50,73] and are entered only for the (001) face. Surface energies differ somewhat from those previously calculated[3] where neither self-consistency nor relaxation were taken into account. The agreement with experiment and DFT is still good. We now summarize the results and trends exhibited in the Tables I–VI. We will then illustrate the important trends graphically.

TABLE I. Interlayer separations Δd_{ij} and surface energies γ for the low index faces of Ni as calculated by the NRL-TB, other methods, and experimental measurements.

Atom-Face	NRL-TB	DFT	EAM	MEAM	Expt.
Ni (001)					
Δd_{12} (%)	−1.0	−3.6[a]	−3.0[c]	2.5[d]	−3.2±.5[e] −1±1[f]
Δd_{23} (%)	0.0	1.4	−0.4	0.1	0±1
Δd_{34} (%)	−0.3	0.3	0.0	0.0	
γ(J/m^2)	3.33	2.43[b]	1.58	2.42	2.38[g]
Ni (011)					
Δd_{12} (%)	−6.6	−10.3[a]	−7.0[c]	−3.1[d]	−8.7±.5[h]
Δd_{23} (%)	4.4	3.2	1.8	3.9	3.0±.6
Δd_{34} (%)	−0.5	0.0	−1.0	−0.3	−0.5±.7
γ(J/m^2)	3.43	2.37[b]	1.73	2.37	
Ni (111)					
Δd_{12} (%)	1.8	−0.9[a]	−1.9[c]	2.7[d]	−1.2±1.2[e]
Δd_{23} (%)	0.3	0.0	0.0	0.1	
Δd_{34} (%)	−0.1	0.0	0.0	0.0	
γ(J/m^2)	2.92	2.01[b]	1.45	2.02	

[a]Local-spin-density-functional theory (LSDF), ultrasoft pseudopotentials (USP)(Ref. 52).
[b]Local-density approximation (LDA), full charge density (FCD) linear muffin-tin orbitals (LMTO) (Ref. 61).
[c]Embedded atom method (EAM) (Ref. 47).
[d]Modified embedded atom method (MEAM) (Ref. 49).
[e]Rutherford backscattering spectroscopy (RBS) (Ref. 43).
[f]Low-energy-electron diffraction (LEED) (Ref. 32).
[g]Experimental determination for an average face (Ref. 73)
[h]LEED (Ref. 33).

The TB results in Table I are for paramagnetic Ni. A magnetic TB parametrization exists, but self-consistency has not yet been built into the NRL-TB code when spin-dependent interactions are included. The DFT calculation[52] for the interlayer spacings does include spin dependence. The results for Ni exhibits several trends that persist for most of these fcc metals: (1) The surface energies are somewhat above the DFT values (while EAM is usually too low). (2) The interlayer spacing d_{12} is less contractive (or more expansive) than the DFT results (while EAM has too much contraction). (3) The face-to-face and layer-to-layer variations in the interlayer spacings are close to those of DFT.

In Table II the "EAM" results for Rh are actually for the molecular dynamics/Monte Carlo effective medium theory.[48] No present theory accounts for the observed[35] first interlayer expansion d_{12} for Rh(001), a discrepancy that persists to Pd(001) as well. The TB surface energies are very close to the DFT results, whereas the interlayer spacings are slightly

TABLE II. Interlayer separations Δd_{ij} and surface energies γ for the low index faces of Rh as calculated by the NRL-TB, other methods, and experimental measurements.

Atom-Face	NRL-TB	TB		DFT		EAM	MEAM	Expt.
Rh (001)								
Δd_{12} (%)	−2.2			−3.5[a]	−3.0[b]	0.0[c]	−4.1[d]	1.0±.9[e]
Δd_{23} (%)	−0.2				−0.1	0.0		
Δd_{34} (%)	0.3							
γ(J/m^2)	3.08	3.43[f]	3.08[g]	3.12[h]	2.80[i]	2.88	2.60[j]	2.59[k]
Rh (011)								
Δd_{12} (%)	−4.9			−7.5[a]	−9.2[b]	−4.2[c]		−6.9±1.2[l]
Δd_{23} (%)	−1.0				2.1	0.5		1.9±1.0
Δd_{34} (%)	2.7							
γ(J/m^2)	3.18	3.72[f]	3.29[g]	3.22[h]	2.90[i]	3.12	2.92[j]	
Rh (111)								
Δd_{12} (%)	−1.0				−2.5[a]	−1.0[c]	−2.1[d]	−1.6±.8[e]
Δd_{23} (%)	−0.8					0.0		
Δd_{34} (%)	0.1							
γ(J/m^2)	2.79	3.26[f]	2.84[g]	2.65[h]	2.48[i]	2.73	2.60[j]	

[a]LDA, full potential (FP)-LMTO (Ref. 53).
[b]Generalized gradient approximation (GGA) (Ref. 54).
[c]Molecular dynamics/Monte Carlo corrected effective medium (MD/MC-CEM) theory (Ref. 48).
[d]MEAM (Ref. 15).
[e]LEED (Ref. 35).
[f]Tight-binding (TB) approximation (Ref. 28).
[g]Tight-binding (TB) approximation (Ref. 21).
[h]LDA, Korringa–Kohn-Rostoker (KKR) method (Ref. 57).
[i]LDA, FCD-LMTO (Ref. 61).
[j]MEAM (Ref. 50).
[k]Extrapolation of experimental data to 0 K—average face (Ref. 50).
[l]LEED (Ref. 36).

higher (less contractive) than experiment, whereas DFT errs in the opposite sense from experiment. The agreement with experiment is generally better for the TB spacings than for DFT, although we have no explanation for this. Two other TB calculations for the surface energy are shown[21,28], one of which[21] gives surface energies in close agreement with NRL-TB and DFT.

Table III exhibits the same anomaly with respect to d_{12} of the (001) face for Pd as occurs for Rh(001). Even the DFT results, which are full-potential calculations,[53] seriously underestimate the experimental spacing. We will return to this point later when we discuss the figures. Overall, the NRL-TB surface energies and interlayer spacings agree best with DFT for Pd of the metals studied. Also, the NRL-TB surface energies are almost the same as the TB calculation of Ref. 21.

In Table IV the agreement is good between the TB Ir surface energies and the full-potential DFT results.[57,61] There is also reasonable agreement for the (001) and (011) interlayer spacings between TB and DFT (which are pseudopotential LDA).[55] The main discrepancy is for the (111) face where, typically, the TB predicts a slight expansion, whereas DFT predicts slight contraction. The (001) and (011) surfaces of Ir reconstruct at absolute zero to room temperature, as do the corresponding surfaces of Pt and Au, thus experiments on the 1×1 are difficult to perform. [Here, also, the measurement on the (111) has a large error].[34]

The same caveat regarding reconstruction and comparison with experiment holds for Pt as well (Table V), except this applies to the (111) face as well. While the TB surface energies agree fairly well with DFT, especially with regards to the variation with face, the interlayer spacings are significantly different. All these comparisons are for the experimentally inaccessible 1×1 surfaces. The structure of the "missing row" (011) reconstruction has been treated extensively both experimentally[40,42] and theoretically.[46,51,58] We will see very good agreement between TB, DFT and experiment when we consider (011) reconstructions.

The above remarks concerning Pt largely pertain also to Au (Table VI). Here, however, the TB Au(011) interlayer spacings are in good agreement with DFT. We will also see that the structure of the (011) missing row reconstruction is in good agreement with DFT and experiment.

We plot in Fig. 1 the (001) surface energy for the different metals to illustrate the trends between different metals and different methods. The most meaningful comparison would be between our TB method results and DFT calculations. Except for Ir, the DFT (001) surface energies are very close to the experiments with polycrystalline samples. Since the surface energies of fcc metals usually follow the trend

TABLE III. Interlayer separations Δd_{ij} and surface energies γ for the low index faces of Pd as calculated by the NRL-TB, other methods, and experimental measurements.

Atom-Face	NRL-TB	TB	DFT		EAM	MEAM	Expt.
Pd (001)							
Δd_{12} (%)	−2.0		−0.6[a]		−4.9[b]	−2.0[c]	3.1±1.5[d]
Δd_{23} (%)	0.7				0.2	0.2	
Δd_{34} (%)	−0.5					0.0	
γ(J/m^2)	1.85	1.78[e]	2.22[f]	2.33[g]	1.37[h]	1.66	2.00[i]
Pd (011)							
Δd_{12} (%)	−5.4		−5.3[a]		−11.2[b]	−11.2[c]	−6.0±2[j]
Δd_{23} (%)	3.2				2.5	4.4	1.0±2
Δd_{34} (%)	3.8					−0.6	
γ(J/m^2)	2.02	2.00[e]	2.39[f]	2.23[g]	1.49[h]	1.67	
Pd (111)							
Δd_{12} (%)	−0.1		−0.1[a]		−3.2[b]	−0.3[c]	−0.9±1.3[k]
Δd_{23} (%)	0.5				0.3	0.0	
Δd_{34} (%)	0.0					0.0	
γ(J/m^2)	1.67	1.69[e]	2.01[f]	1.92[g]	1.22[h]	1.38	

[a]LDA, FP-LMTO (Ref. 53).
[b]EAM (Ref. 47).
[c]MEAM (Ref. 49).
[d]LEED (Ref. 37).
[e]Tight-binding (TB) approximation (Ref. 21).
[f]LDA, KKR (Ref. 57).
[g]LDA, FCD-LMTO (Ref. 61).
[h]EAM (Ref. 45).
[i]Experiment—average face (Ref. 73).
[j]LEED (Ref. 38).
[k]LEED (Ref. 34).

$$\gamma(011) > \gamma(001) > \gamma(111), \tag{1}$$

this may not be surprising since in some sense the (001) face would be the "average" face. The TB method does a good job reproducing the DFT results for variations in surface energy among different metals. The MEAM, likewise, reproduces these trends rather well, whereas the EAM, as is well known, usually significantly underestimates surface energies. However, there are many versions of the EAM and related methods (SEAM,[14] glue model,[74] effective medium theory[48,75]) that give rather widely varying surface characteristics. While some of these methods are specifically fitted to surface data, the EAM's represented in Fig. 1 are not. Note that the EAM cannot directly be applied to Ir because this method is incapable of reproducing the negative Cauchy ratio in the elastic constants that is experimentally observed, while the TB method does yield a negative Cauchy ratio.[3] Except for Ni, the TB (001) surface energies are within 25% of the DFT predictions. The tendency is for the TB surface energies to be above the DFT results unless the *d*-shell is almost completely filled (Pd and Au), in which case the surface energies are slightly below the DFT values. The DFT and TB results are very close for Rh, Ir, and Au, with the maximum disagreement with DFT of 37% for Ni.

To examine the trends between different faces we plot in Figs. 2–4 the face-dependence of the surface energies for Pd, Ir, and Au, respectively. The surface energy differences among the three faces here arise mainly out of the differences in the coordination of surface atoms, with (011) the least coordinated [five missing nearest neighbors (NN)], (001) next (four missing NN), and (111) the most coordinated (three missing NN). This usually accounts for the trend of Eq. (1). The EAM almost always reproduces this ordering; the DFT, TB, and MEAM results, however, occasionally deviate from this trend. For Ir the DFT result of Ref. 61 predicts $\gamma(001) > \gamma(011)$, while the DFT result of Ref. 57 yields the usual ordering $\gamma(001) > \gamma(011)$. In this case TB gives $\gamma(001) > \gamma(011)$. A similar disagreement in the two DFT results[57,61] occurs for Pd, with the TB method closely reproducing the face-to-face variations of Ref. 57. Overall, the TB method gives a better description of the DFT face-to-face variation than the other semiempirical methods.

Since the EAM is basically a spherically symmetric theory, with covalent bonding described in an angle-independent way, the simple monotonic ordering with coordination is expected. The MEAM has an angular dependence that is fit empirically. The TB method has an underlying basis of atomic orbitals and a bonding-antibonding concept (hopping integrals), which the other semiempirical methods do not have. This complicates the angular dependence and the dependence on coordination, but brings it into closer resemblance to density functional theory. Overall, we conclude

TABLE IV. Interlayer separations Δd_{ij} and surface energies γ for the low index faces of Ir as calculated by the NRL-TB, other methods, and experimental measurements.

Atom - Face	NRL-TB	DFT	EAM	MEAM	Expt.
Ir (001)					
Δd_{12} (%)	−2.0	−3.8[a]		−4.8[b]	-3.6 ∓ 5[c]
Δd_{23} (%)	−0.4	1.0			
Δd_{34} (%)	0.4	−0.5			
γ(J/m^2)	3.98	3.71[d] 3.72[e]		2.91[f]	3.00[g]
Ir (011)					
Δd_{12} (%)	−11.7	−11.6[a]			
Δd_{23} (%)	4.8	5.4			
Δd_{34} (%)	1.0	−1.3			
γ(J/m^2)	3.98	3.82[d] 3.61[e]		3.06[b]	
Ir (111)					
Δd_{12} (%)	0.9	−1.3[a]		−4.8	-2.6 ∓ 4.5[c]
Δd_{23} (%)	−0.9	−0.2			
Δd_{34} (%)	0.2	0.0			
γ(J/m^2)	3.45	3.02[d] 2.97[e]		2.84[f]	

[a]LDA, smooth, norm-conserving pseudopotentials (Ref. 55).
[b]MEAM (Ref. 15).
[c]LEED (Ref. 34).
[d]LDA, KKR (Ref. 57).
[e]LDA, FCD-LMTO (Ref. 61).
[f]MEAM (Ref. 50).
[g]Extrapolation of experimental data to 0 K—average face (Ref. 50).

that the TB method predicts the face-to-face variations in surface energy because of a realistic treatment of the angular degrees of freedom and coordination. We will revisit this provisional conclusion when we consider surface relaxation.

In Figs. 5–7 we plot the interlayer relaxation Δd_{12} for the (001), (011), and (111) faces for the different metals and methods. We also show the TB results when charge transfer to the surface is not handled self-consistently (TB-NSC). Most of the TB-NSC results show unrealistically large interlayer expansions. Most of the (011) results for TB-NSC are not shown because they are off-scale with expansions of more than 7%. The large effect of charge self consistency on interlayer spacings parallels its well-established importance in other TB investigations, originally demonstrated in the calculation of the properties of binary alloys[76] and surface magnetism.[77] Experimental points are also shown, with their size indicating the experimental error. All the methods, except DFT, for Ni are for paramagnetic Ni, whereas in reality it is ferromagnetic. The Ir, Pt, and Au all have quasihexagonal low temperature (001) reconstructions and (011) missing row reconstructions. Au and Pt (111) surfaces have low temperature reconstructions as well. The indicated experimental points are for the unreconstructed 1×1 structures. As previously noted, where reconstruction occurs the experimental measurements for the 1×1 surface[34] may be difficult and unreliable. We will consider in Sec. III B the interatomic relaxations of the Au, Pt, and Ir (011) missing row structure, where careful measurements have been made.[40–42,44]

The interlayer expansions of Pd(001) and Rh(001) have also attracted a lot of attention over the past decade. None of the methods, including DFT,[53,54]predict the observed[35,36] first interlayer expansion. Surface magnetism,[30,37,78] finite temperature effects,[78,79] and the role of repulsive *d*-wave interactions for nearly filled *d*-shells[24,25] have been considered as possible reasons for the discrepancies, which have yet to be resolved.

Overall, the TB method produces less interplanar contraction (or more expansion) than DFT or experiment (whereas the EAM produces more contraction). It has long been established that pair interatomic potentials lead to first interlayer expansion (positive Δd_{12}).[80] The EAM, which is mainly sensitive to the number of missing bonds, typically leads to negative Δd_{12}. The TB method predicts relaxations of both signs [for (001) and (111)], as does experiment. DFT, with a few exceptions, predicts a negative Δd_{12} that is slightly lower than the experimental measurements.

The overall agreement with experiment and DFT is slightly better for TB than for the other methods, and significantly better in metal-to-metal trends. The metal-to-metal trends reflect the roles of different orbital configurations on the expansion or contraction of the interlayers. However, the precise nature of these roles is very complex. For example, the sequences Rh-Pd and Ir-Pt-Au correspond to increased *d*-shell filling. The DFT and experimental measurements on the (001) faces indicate increasing Δd_{12} along these sequences. Studies based on TB theory do, indeed, indicate that the *d*-wave contribution to the relaxation force on (001) surface atoms becomes repulsive when the *d*-shell is nearly filled.[24,25] A similar effect has also been suggested for *s*-waves.[81] The metal-to-metal variations produced by the TB method are similar to the experimental and DFT variations, except for Pt (011). We tentatively conclude that the TB method describes the metal-to-metal relaxation trends because it contains a realistic angular dependence, such as the repulsive *d*-wave feature for (001) surfaces.

Figures 8–11 show the interplanar spacing relaxation Δd_{12} for the three low-index faces for Ni, Rh, Pd, and Au, respectively. Except for the aforementioned experimental anomalies for Rh and Pd (001), and the MD/MC-CEM result[48] for Rh(001) and (111), all methods and experimental measurements indicate $\Delta d_{12}(011) < \Delta d_{12}(001) < \Delta d_{12}(111)$, simply corresponding to the least coordinated surface having more interlayer contraction. The TB relaxations, while slightly less contractive than those of DFT, reproduce well the DFT face-to-face variations.

Another way to test the dependence of a model on different coordination and geometric configurations is to examine the multilayer spacings Δd_{ij}. Fig. 12–15 give the multilayer spacings for the (011) face of Ni, Au, Ir, and Pt, respectively. Figure 14 includes results for Ir(001) as well, but here EAM and MEAM results for the three Δd_{ij}'s are not available. For Ni and Au(011) (Figs. 12 and 13) all methods reproduce the trend $\Delta d_{12} < \Delta d_{34} < \Delta d_{23}$ seen in DFT and experiment. An alteration in the sign of Δd_{ij} is commonly observed in metals. A simple explanation is that the first interlayer contracts to help saturate the dangling bonds of the surface atoms, leading to an oversaturation of the second layer atoms that induces an expansion between layers 2 and 3, etc. The TB method gives a quite good fit to the DFT interlayer spacings on these two surfaces. The Ir(011) TB interlayer spacings

TABLE V. Interlayer separations Δd_{ij} and surface energies γ for the low index faces of Pt as calculated by the NRL-TB, other methods, and experimental measurements.

Atom-Face	NRL-TB	DFT		EAM		MEAM	Expt.
Pt (001)							
Δd_{12} (%)	1.5		−2.6[a]	−4.2[b]	−6.9[c]	−2.1[d]	0.2±1.6[e]
Δd_{23} (%)	−0.5			0.3	0.6	0.2	
Δd_{34} (%)	−0.4			0.0		0.0	
γ(J/m^2)	3.29	2.65[f]	2.73[g]		1.65	2.16	2.49[h]
Pt (011)							
Δd_{12} (%)	−5.7	−11.6[i]	−14.6[j]	−9.4[b]	−17.6[c]	−17.2[d]	
Δd_{23} (%)	−2.5	5.4	8.3	3.0	2.1	8.8	
Δd_{34} (%)	−0.3	−1.6 −1.0			−1.5	0.4	
γ(J/m^2)	3.39	2.91[f]	2.82[g]		1.75	1.99	
Pt (111)							
Δd_{12} (%)	3.5		0.7[a]	−2.7[b]	−4.8[c]	1.1[d]	1.4±.9[e]
Δd_{23} (%)	0.3			0.4	0.8	0.0	
Δd_{34} (%)	−0.3			0.0		0.0	
γ(J/m^2)	2.77	2.31[f]	2.30[g]		1.44	1.65	

[a]GGA, ultra-soft pseudopotentials (USP) (Ref. 15).
[b]EAM (Ref. 47).
[c]EAM (Ref. 45).
[d]MEAM (Ref. 49).
[e]LEED (Ref. 34).
[f]LDA, KKR (Ref. 57).
[g]LDA, FCD-LMTO (Ref. 61).
[h]Extrapolation of experimental data to 0 K–average face (Ref. 50).
[i]LDA, linear combination of atomic orbitals (LCAO) (Ref. 59).
[j]GGA, USP (Ref. 58).

(Fig. 14) are very close to DFT. The DFT d_{ij} ordering for the Ir(001) surface is not reproduced by TB, but the agreement for the individual d_{ij}'s is good. The agreement with DFT is not good for the Pt(011) surfaces. We will shortly reconsider surface relaxation of the Pt(011) surface when we examine its missing row reconstruction where experimental measurements are available.

B. Ir, Pt, and Au(011) missing-row reconstructions

Ir, Pt, and Au form ground state missing row 2×1 reconstructions on their (011) surfaces. Although experimental data for the corresponding 1×1 surfaces is largely lacking, data is available for the missing-row reconstructions.[40–42,44] The reconstructed surface relaxes inplane as well as vertically. Most of these relaxations have been measured experimentally as well as calculated in DFT.[55,58,60,61] The relaxations provide a further testing ground for the TB and other semiempirical methods since they test geometries and coordination combinations different than those of the 1×1 surface.

In a previous publication, one of the authors (M.I.H.) has given a simple explanation of the missing-row (MR) reconstruction.[14] The 2×1 MR reconstruction has a surface layer where only every other close-packed [110] row is occupied. This can be thought of as adding these alternate rows on top of the 1×1 surface, in which case these extra atoms can covalently bond with four nearest-neighbor atoms on the topmost 1×1 surface. The number of missing bonds per unit area is the same for both the 1×1 and 2×1 missing-row structures. However, there are only half the number of the least (sevenfold) coordinated atoms in the 2×1 structure. Since the nature of covalent bonding leads to a contribution to the surface energy that is quadratic in the number of missing bonds,[14] the 2×1 missing-row structure is energetically favorable. Opposing this are the additional 20% missing attractive second neighbors in the MR configuration. Thus the stability of the MR structure depends on a competition between first and second neighbor effects.

Table VII gives TB, EAM, MEAM, DFT, and experimental results, where available, for the atomic relaxations on the 2×1 MR structure. In addition to the vertical relaxations Δd_{ij}, the corrugation of the third layer, b_3, and the pairing distances on the second and fourth layers, p_2 and p_4, appear. The reconstruction energy, $\gamma_R=\gamma(\mathrm{MR})-\gamma(1\times1)$, is also given. The experimental reconstruction energy is negative for all three metals, i.e., MR is the stable phase. (For Ir, the ground state may be $N\times1, N>2$).[41] The definitions of the corrugation and pairing parameters differ from reference to reference: Here b_3 is defined as the difference in height of the highest and lowest atoms of layer 3, and the pairing distances p_2 and p_4 are defined, for the second and fourth layer, respectively, as the change in the distance between the

TABLE VI. Interlayer separations Δd_{ij} and surface energies γ for the low index faces of Au as calculated by the NRL-TB, other methods, and experimental measurements.

Atom-Face	NRL-TB	DFT		EAM		MEAM	Expt.
Au (001)							
Δd_{12} (%)	1.7		−1.0[a]	−6.3[b]	−5.4[c]	−5.8[d]	
Δd_{23} (%)	−0.4			0.1	1.5	1.2	
Δd_{34} (%)	0.1				0.0	−0.2	
γ(J/m^2)	1.31	1.62[e]	1.68[f]	0.92		1.12	1.54[g]
Au (011)							
Δd_{12} (%)	−10.3		−9.8[h]	−15.2[b]	−12.1[c]	−18.0[d]	
Δd_{23} (%)	8.7		7.8	2.2	3.6	6.3	
Δd_{34} (%)	−3.2		−0.8		−1.6	−2.0	
γ(J/m^2)	1.40	1.75[e]	1.70[f]	0.96		0.99	
Au (111)							
Δd_{12} (%)	3.7		−0.1[a]	−4.2[b]	−3.5[c]	−3.2[d]	
Δd_{23} (%)	−2.3			0.6	0.6	0.6	
Δd_{34} (%)	−0.2				−0.1	−0.1	
γ(J/m^2)	1.04	1.39[e]	1.28[f]		0.79	0.87	

[a]LDA, FP-LMTO (Ref. 56).
[b]EAM (Ref. 45).
[c]EAM (Ref. 47).
[d]MEAM (Ref. 49).
[e]LDA, KKR (Ref. 57).
[f]LDA, FCD-LMTO (Ref. 61).
[g]Experimental determination – average face (Ref. 73).
[h]LDA (Ref. 60).

$[\bar{1}10]$ rows centered directly below the missing row and this distance in the 1×1 structure. We have been careful to convert the results of other calculations and experiments to these definitions.

The TB method reproduces the geometric trends of the DFT and experimental measurements for the 2×1 MR reconstructions. The only significant defect is the failure by a very small amount to predict the MR phase of Ir(011) as the ground state. The Δd_{12} values follow the trend Au$<$Pt$<$Ir in both the TB and the DFT results. The pairing distances of TB agree well with DFT and experiment. The very small pairing for Ir(011) of DFT is reproduced by TB. Only the TB third layer corrugation (b_3) is overestimated for Ir and Au compared to DFT. The experimental measurements, where available, follow similar trends to the DFT calculations, except for the very large first interlayer contraction for Ir(011),[41] but this measurement is actually for a 3×1 MR reconstruction. The TB, DFT, and experimental Δd_{23}'s agree in sign, whereas the other semiempirical models give the

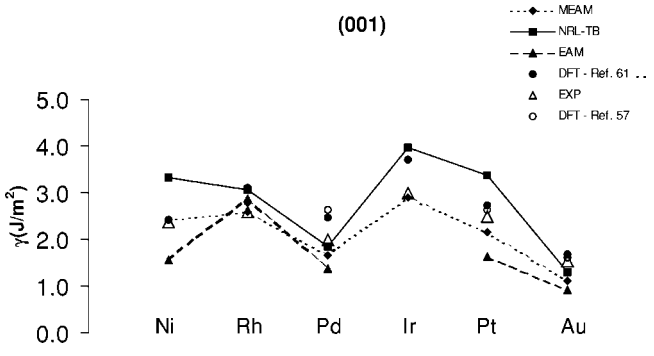

FIG. 1. Surface energies for the (001) face as predicted by the NRL-TB method, other semiempirical methods (EAM, MEAM), and density functional theory. All the numerical values in all the figures are from Tables I–VI unless otherwise noted. The experimental values are polycrystalline averages. The Rh "EAM" result is for the molecular dynamics/Monte Carlo corrected effective medium (MD/MC-CEM) of Ref. 48.

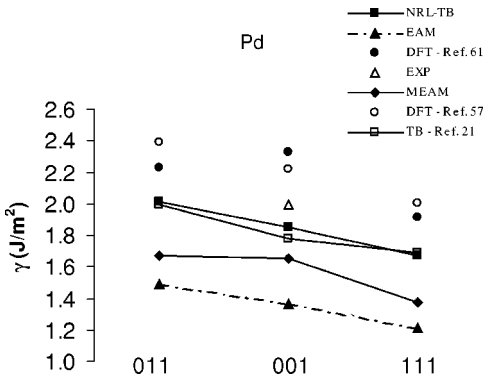

FIG. 2. The dependence of the surface energy on the exposed face for Pd as predicted by NRL-TB, semiempirical methods, and DFT. The experimental point is indicated for the (001) face, but is really for a polycrystalline surface. The TB results in Ref. 21 are also included.

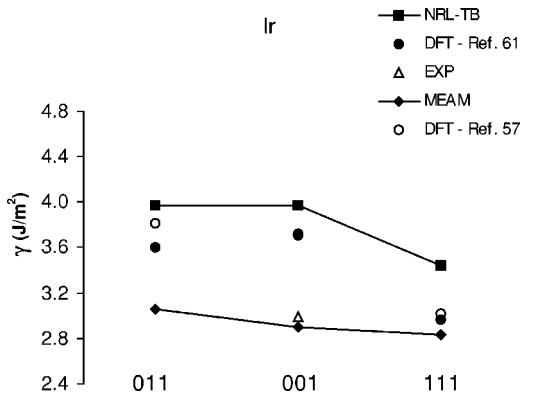

FIG. 3. The dependence of the surface energy on the exposed face for Ir as predicted by NRL-TB, MEAM, and DFT. The experimental point is for a polycrystalline surface.

wrong sign. Curiously, except for Δd_{12}, the TB atomic relaxations for Pt(011) are closer to agreement with experiment than the DFT predictions. This is likely not attributable to the inclusion of 16 layers in the TB calculation versus the inclusion of only eight in the DFT calculation,[58] as we have carried out TB calculations of these relaxations for 7, 9, 11, 13, and 16 layers with these relaxations being reasonably well converged even at seven layers. Neither is the use of only six k points (we use 216) in Ref. 58 the source of any significant error as we examined the sensitivity of the TB results as a function of the choice of k points. The maximum error due to layer or k point truncation is about 1% for the Δd_{ij}'s, and about 0.01 Å for the lateral relaxation quantities. A remaining source of disagreement could be the different approximation schemes employed within DFT [e.g., use of LAPW versus pseudopotentials (as in Ref. 58), and treatments of exchange and correlation other than the Hedin and Lundqvist prescription that we are using] between those used to fit the TB parameters and those used by other investigators in the referenced surface calculations. Moreover, the TB missing-row relaxations agree very well with DFT and experiment.

IV. DISCUSSION

The results of the preceding section indicate that the TB method gives generally reliable predictions of surface energies, relaxations, and reconstructions. We attribute this success to the angular and bonding-antibonding degrees of freedom of this method that are missing in the other nonquantum-mechanical approaches. We now examine this aspect of the TB method more closely to assess how realistically it describes the interaction of atoms in the bulk and surface environments. To do this we analyze the contributions to the energy from various terms of the TB method.

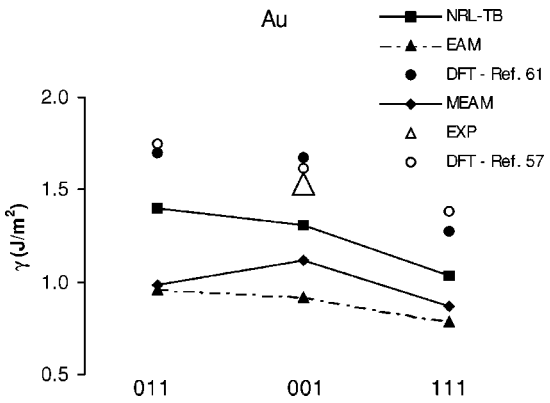

FIG. 4. The dependence of the surface energy on the exposed face for Au as predicted by NRL-TB, semiempirical methods, and DFT. The experimental point is for a polycrystalline surface.

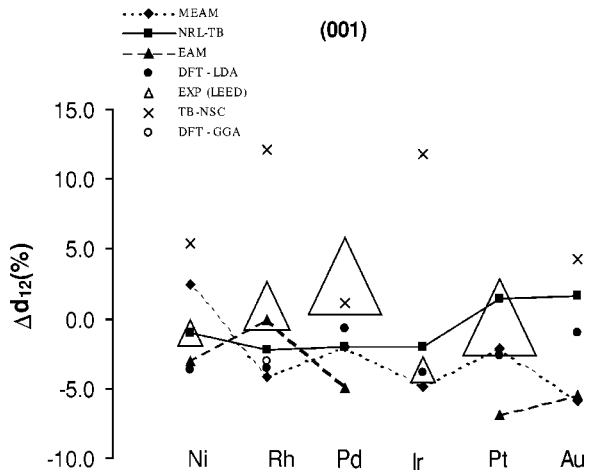

FIG. 5. The interlayer separations of the top two layers on the (001) surfaces as predicted by different methods and experimental LEED measurements. The interlayer separations are expressed as their deviations (Δd_{12}) from those in the unrelaxed bulk. The "EAM" results for Rh are MD/MC-CEM calculations (Ref. 48) and the DFT results for Rh are from Refs. 53 (LDA) and 54 (GGA). The TB results when charge self-consistency is not included (TB-NSC) is indicated.

The total energy of the system in the TB method is $\mathrm{Tr}(\rho H)$, where ρ is the density matrix and H the Hamiltonian matrix, where the decomposition of this quantity can be written

$$E = \mathrm{Tr}(\rho H) = \sum [\rho]_{i\alpha,j\beta}[H]_{j\beta,i\alpha}, \tag{2}$$

where the summation is over atom labels i,j and state labels α,β, and implicitly includes an integral over $\mathbf{k}$ as well. The

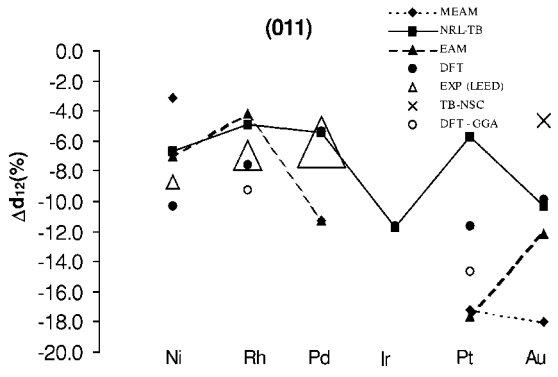

FIG. 6. The interlayer separations of the top two layers on the (011) surfaces as predicted by different methods and experimental LEED measurements. The interlayer separation notation and the remarks about Rh EAM results and TB-NSC results are the same as in Fig. 5. GGA results also appear for Rh and Pt.

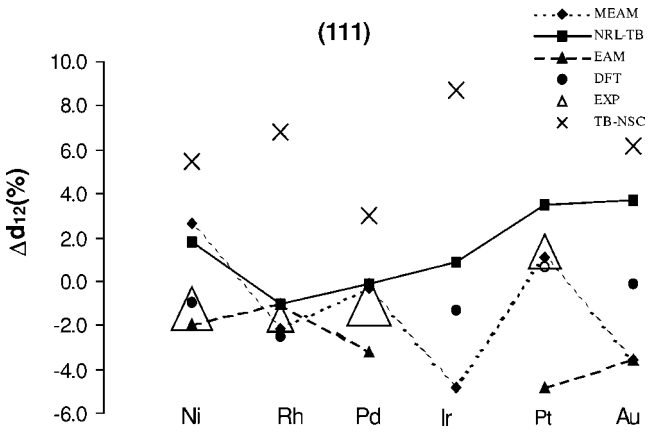

FIG. 7. The interlayer separations of the top two layers on the (111) surfaces as predicted by different methods and experimental measurements. The open circle for Pt is the GGA result. The interlayer separation notation and the remarks about Rh EAM results and TB-NSC results are the same as in Fig. 5.

expression for the Hamiltonian matrix is given in Eq. (3) of Ref. 8. We define an effective bond energy between nearest neighbor (NN) atoms i and j from states α and β as the corresponding contribution to Eq. (2). We have calculated these individual contributions for both the bulk and for the (001) surfaces.

Figure 16 gives the effective bond energy contributions to the bulk systems of the fcc metals we have investigated. We also include TB calculations for Mo and W to contrast results obtained for the fcc metals near the end of the 4*d* and 5*d* sequences with those near the middle of the same sequences (Mo and W, respectively). Although these metals have a ground state bcc structure, our calculations were carried out for fcc at the equilibrium lattice constant for this structure. In the bulk the contributions are independent of the particular NN, and the results shown are further summed over all states with a common s,p, or d label (e.g., $pp \rightarrow p_x p_x + p_x p_y + p_x p_z + p_y p_y + p_y p_z + p_z p_z$, etc.). In this figure the *ss*, *sp*, *pp*, and *dd* effective bond energies are shown. The

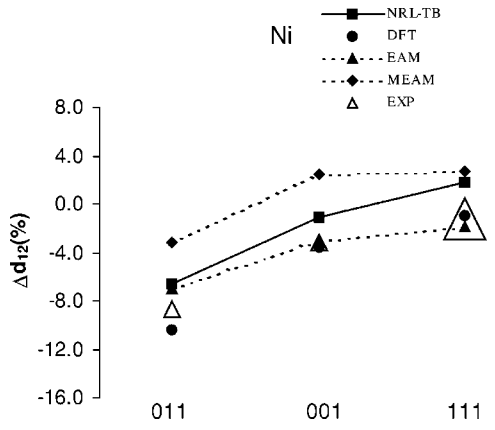

FIG. 8. The interlayer separations of the top two layers for the low-index faces of Ni as predicted by different methods and experimental measurements. The experimental (001) and (111) points are RBS measurements (Ref. 43), and the (011) point is LEED (Ref. 33).

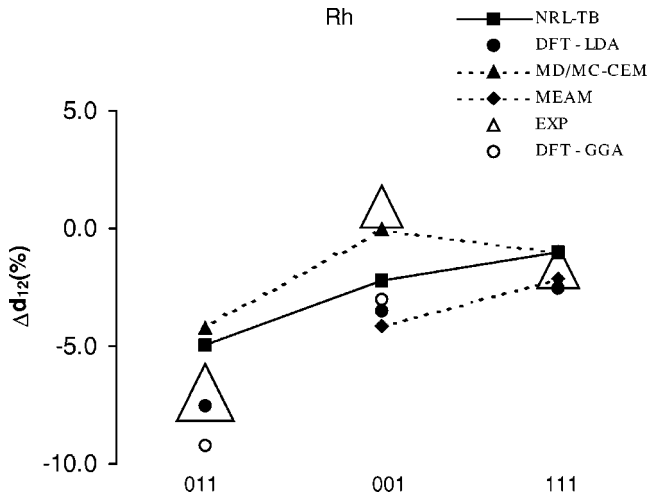

FIG. 9. The interlayer separations of the top two layers for the low-index faces of Rh as predicted by different methods and experimental measurements.

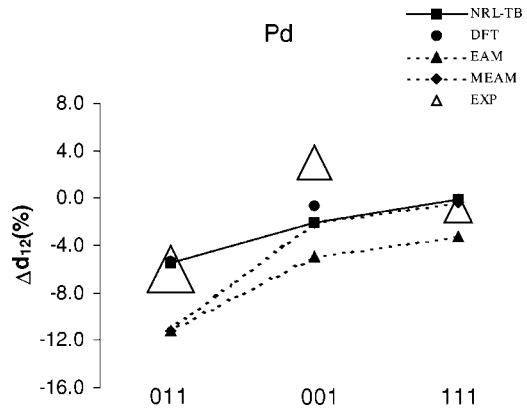

FIG. 10. The interlayer separations of the top two layers for the low-index faces of Pd as predicted by different methods and experimental measurements.

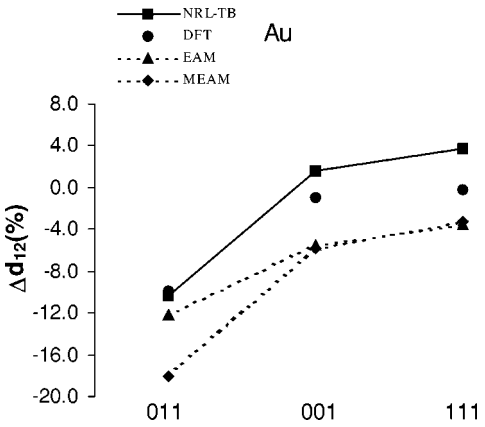

FIG. 11. The interlayer separations of the top two layers for the low-index faces of Au as predicted by different methods.

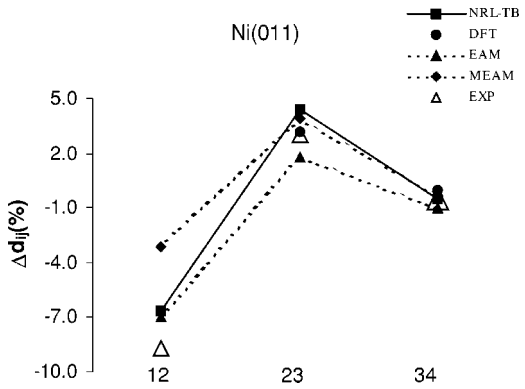

FIG. 12. The interlayer separations of the top four layers of Ni (011) as predicted by different methods and experimental measurements.

other contributions can be significant, but do not sharply vary from metal to metal.

In Fig. 16 we notice that the attraction of the *dd* bond strengths decreases greatly from the middle of the *d* shells to the end, even becoming antibonding for Pd, Pt, and Au. This is the expected behavior of *d* states across the second halves of the *d* shells as bonding and then antibonding states are successively filled.[55,82] The *ss* and *sp* terms have a tendency to increase in attraction across the *d* shells (except for *sp* for Au), and increasingly are responsible for the binding of the crystal as the *d* waves lose their attraction. This, again is the expected behavior demonstrating the reasonable angular and bonding-antibonding behavior of the TB method at least in the bulk.

One of the more interesting and controversial issues for fcc metal surfaces is the origin of the low-index surface reconstructions for the late 5*d* metals Ir, Pt, and Au. All three low-index faces reconstruct at low to room temperature for the latter two, while the (011) and (001) faces reconstruct for Ir. The (001) reconstructions are "quasihexagonal" where the surface layer takes on a structure very similar to a (111) face. Both the (111) and (001) reconstructions are characterized by an increased density of surface atoms, with a loss of symmetry with the underlying substrate, whereas the (011) reconstruction is normally a 2×1 "missing row" reconstruction where only every other $[\bar{1}10]$ nearest neighbor row on the

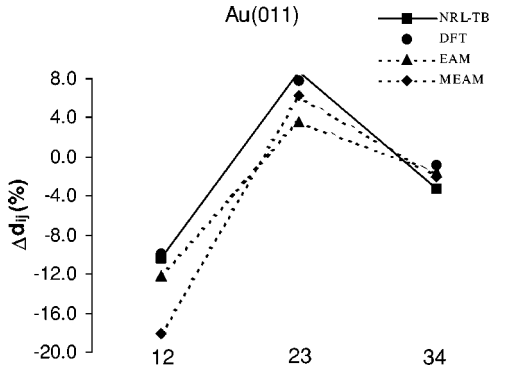

FIG. 13. The interlayer separations of the top four layers of Au (011) as predicted by different methods. The EAM results are from Ref. 47.

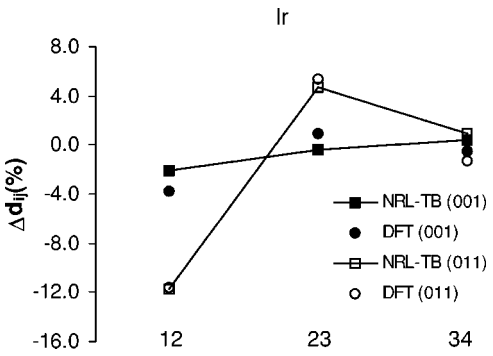

FIG. 14. The interlayer separations of the top four layers of Ir (001) and Ir (011) as predicted by the NRL-TB method and DFT.

top layer is occupied, but otherwise, there is no loss of symmetry with the substrate.

The controversy regards the "driving force" of the reconstructions. Surface stress (or "surface stress relief ") is often invoked as these metals have large tensile surface stress compared to, say, their late 4*d* counterparts, and there is a surface energy reduction associated with the work of tensile surface stress when surface density increases.[63,82–84] An alternate explanation, at least for (001) and (011) reconstructions, is the lower surface energy of the (111) face, because of higher coordination, than the (001) and (011) faces. In this picture the (001) surface will take on the (111)-like quasihexagonal reconstruction if the (111)–(001) surface energy reduction more than offsets the gain due to loss of registry with the substrate. On (011) the missing row reconstruction can be approximated as faceting into (111) faces, and if the surface energy loss by exposing (111) faces can offset the gain from the increased area of exposed surface, this reconstruction will occur.[55] (Relaxation also plays a role here.) In Tables II–VI both the TB and DFT predict that these surface energy differences are considerably larger for the 5*d* metals Ir and Pt than they are for 4*d* Rh and Pd. (These surface energy differences are very slightly higher for Rh than for Au.)

Both explanations of the driving force for reconstruction involve surface energy losses by the increased density of surface atoms. It is a general feature of covalent bonding that the bonds strengthen in low coordination environments such as the surface. A strengthening of the surface bonds will lead to more tensile surface stress and to a greater loss of surface

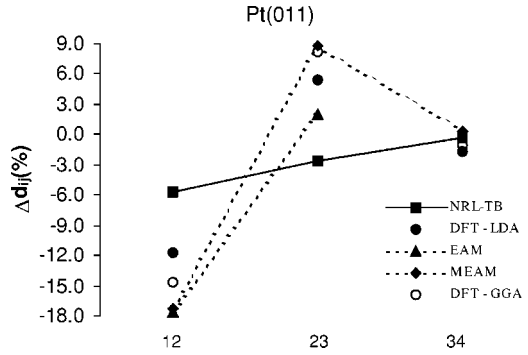

FIG. 15. The interlayer separations of the top four layers of Pt (011) as predicted by different methods.

TABLE VII. (011) 2×1 missing-row relaxation parameters and reconstruction energy as calculated by the NRL-TB, other methods, and experimental measurements.

Metal	NRL-TB	DFT	EAM	MEAM			Expt.
Ir (011)							
Δd_{12} (%)	−11.5	−8.4[a]					−32.0[b]
Δd_{23} (%)	−6.8	−3.3					
Δd_{34} (%)	5.5	2.1					
b_3(Å)	0.292	0.105					
p_2(Å)	−0.019	−0.028					−0.022
p_4(Å)	−0.031						
γ_R(J/m^2)	0.02	−0.05		−0.05[c]	0.13[d]		<0
Pt (011)							
Δd_{12} (%)	−14.3	−16[e]	−17.6[f]		−23.2[g]	−17.4[h]	−16±3[i]
Δd_{23} (%)	2.4	0	−5.1		−2.6	1.1	4±3
Δd_{34} (%)	1.0	2	−0.7				
b_3(Å)	0.21	0.27	0.11		0.29	0.17	0.10
p_2(Å)	−0.12	−0.06	−0.05		−0.12	−0.10	
p_4(Å)	−0.11	−0.14	0.08			−0.10	
γ_R(J/m^2)	−0.12	−0.14	−0.05		−0.48	<0	
Au (011)							
Δd_{12} (%)	−23.0	−17.9[j]	−9.0[k]		−16.7[g]	−20.2[h]	−22.2[l]
Δd_{23} (%)	5.0	3.4	−7.1		−6.6	1.8	
Δd_{34} (%)	0.4	2.0					
b_3(Å)	0.34	0.25	0.12		0.23	0.24	
p_2(Å)	−0.13	−0.08	−0.08		−0.02	−0.14	−0.10
p_4(Å)	−0.14	−0.10				−0.10	
γ_R(J/m^2)	−0.16	−0.08	−0.04	−0.01 [m]	−0.05	<0	

[a]LDA, smooth, norm-conserving pseudopotentials (Ref. 55).
[b]Low-energy ion scattering (LEIS) (Ref. 41).
[c]MEAM (Ref. 15).
[d]MEAM of Ref. 50 calculated in Ref. 15.
[e]GGA, USP (Ref. 58)
[f]EAM (Ref. 46).
[g]MEAM (Ref. 51).
[h]LEED (Ref. 40).
[i]Medium-energy ion scattering (MEIS) (Ref. 42).
[j]LDA (Ref. 60).
[k]Surface embedded atom method (SEAM) (Ref. 14).
[l]X-ray diffraction (XRD) (Ref. 44).
[m]Extended embedded atom method (Ref. 69).

energy of the (111) surface relative to those of (001) and (011) due to the greater density of surface bonds on this surface, which tends toward favoring the reconstructed surfaces.[82] Figure 17 displays the difference between the unrelaxed (001) surface bond strengths and those in the bulk. (Relaxation alters these results very little). These differences are distinguished between intralayer (in-plane) bonds [Fig. 17(a)] and interlayer (between layers 1 and 2) bonds [Fig. 17(b)]. In Fig. 17 the *dd* contributions account for most of the element-to-element variation in the out-of-plane and in-plane bond strengthening. While the *dd* bonds strengthen both in-plane and out-of-plane bonds in the middle of the *d* sequences, near the end of the sequences they strengthen the in-plane bonds but weaken the out-of-plane bonds. The in-plane strengthenings are greater for the late 5*d* metals than for the late 4*d*, and the *ss* and *sp* in-plane strengthenings are also greater for the 5*d* metals. Thus the systematics of the TB method account for the greater propensity for the late 5*d* metals to reconstruct. The role of the loss of the antibonding characteristic of *d* waves at the surface of late 4*d* and 5*d* metals in reconstruction has been suggested in previous works.[55,82]These investigators also attribute the reconstruction of the 5*d* metals to a relativistic contraction of the (hybridized) s*p* orbitals, leading to a greater conversion of the antibonding *d* orbitals to bonding *sp* at the surface. With the exception of Au, the 5*d* metals exhibit stronger *sp* attraction even in the bulk [Fig. 17(a)]. The *ss*, *sp*, and *dd* terms all contribute to the strengthening of the 5*d* intralayer bonds

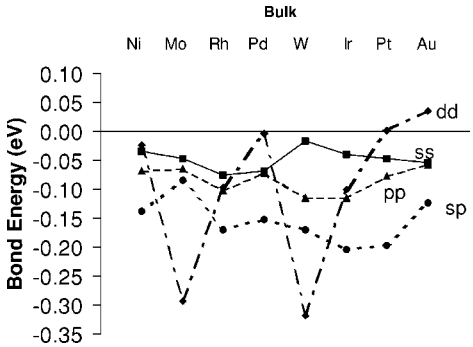

FIG. 16. The *ss*, *sp*, *pp*, and *dd* contributions to the effective bond energies for the fcc structures of various metals in the bulk. Here Ni is a 3*d* metal, whereas the sequence Mo, Rh, and Pd represents increasing filling of the 4*d* shell, and W, Pt, and Au successive filling of the 5*d* shell.

compared to 4*d*. (In Au, *pd* gives a substantial contribution to the bond strengthening to help account for the reconstruction of its surfaces.)

Another interesting feature of Fig. 17 is that, unlike the case for in-plane bonds, the *d* waves weaken the out-of-plane bonds late in the 4*d* and 5*d* sequences [Fig. 17(b)]. This feature has been cited previously as a possible explanation[24,25] of the experimental (001) interlayer expansion[35,37] in Pd and Rh. However, no full TB or semiempirical model,[15,47–49] nor any DFT calculation,[53,54] predicts an actual interlayer expansion. The *s* and *p* contributions here more than compensate for increase in interlayer repulsion due to *d*-states, and perhaps these contributions should not be so attractive. In Au, where the TB method predicts a (001) interlayer expansion, perhaps the *s* and *p* contributions should be less repulsive. Nevertheless, our decomposition of the TB contributions to the bulk and surface bond strengths points to a realistic behavior across the *d* sequences and also in the differences between 4*d* and 5*d* metals. These account for most of the surface energy, surface reconstruction, and surface relaxation trends observed in these metals.

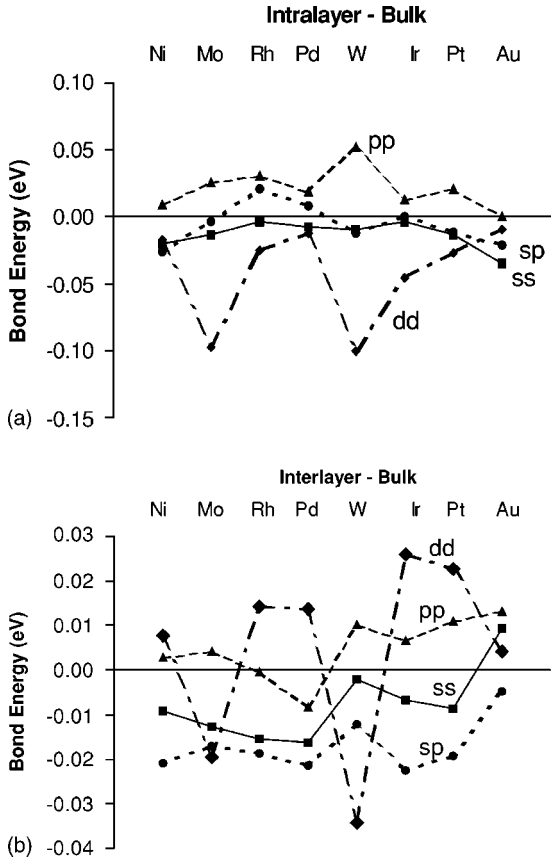

FIG. 17. The *ss*, *sp*, *pp*, and *dd* contributions to the differences between the surface intralayer (a) and interlayer (b) effective bond energies and those in the bulk for the fcc structures of the metals in Fig. 16.

V. SUMMARY AND CONCLUSIONS

We have carried out an extensive survey of the surface properties for the six fcc metals Ni, Rh, Pd, Ir, Pt, and Au using the TB method. In so doing we have tested the transferability of the NRL-TB method to the surface environment and its performance *vis a vis* other semiempirical methods in comparison to DFT and experimental measurements. We have examined the surface energies and interlayer relaxations with regards to trends among different metals, trends among the different low index faces, and the relaxation trends for interlayer distances as one proceeds deeper below the surface.

Generally, the TB predicts surface energies reasonably close to DFT results, with a tendency to err on the high side rather than on the low side as for the other semiempirical methods. The surface energies tend to be closer to DFT when the *d* shell is more completely filled, and better for 5*d* metals than 3*d* or 4*d*. The TB reproduces the metal-to-metal and face-to-face orderings of the surface energies found in DFT significantly better than the other semiempirical methods. The tendency in DFT for the surface energy to decrease as the *d* shells become more filled, or as one proceeds from the (011) to (001) to (111) face, is reproduced in TB predictions. We attribute the realistic metal-to-metal and face-to-face results of the TB method to the realistic treatment of the angular and quantum-mechanical degrees of freedom in the TB formalism.

As in many past TB studies, the self-consistent treatment of charge transfer to the surface is essential. Without it, the TB method often predicts far too much interlayer expansion. Generally, the TB method gives somewhat better surface relaxations than the other semiempirical methods when compared to DFT or experiment. However, the improvement over these methods is not great for individual geometric structural quantities. For any given interlayer relaxation the TB method may or may not do better than the EAM or MEAM, but the metal-to-metal and face-to-face trends are well predicted by the TB method.

The TB method predicts the increased interlayer repulsion with *d*-shell filling, seen in both DFT calculations and experimental measurements. [However, all methods and DFT fail to predict the interlayer expansion experimentally observed for Rh(001) and Pd(001)]. All methods

give reasonable face-to-face variations, typically with $\Delta d_{12}(011) < \Delta d_{12}(001) < \Delta d_{12}(111)$,which is true of the DFT results and experiment [except for Rh and Pd(001)]. In this respect TB gives variations very close to DFT for nearly closed-*d*-shell Pd and Au. Again, we attribute the success of the TB method in describing the metal-to-metal and face-to-face trends to its description of angular forces and bonding-antibonding features.

The TB method also gives good results when compared to DFT and to experiment for relaxations of deeper layers down to Δd_{34}. One notable exception is Pt(011) (1×1). The NRL-TB method, however, gives very good agreement with DFT and experimental measurements for the in-plane and interlayer relaxations of the stable reconstructed missing-row reconstructions of Ir, Pt, and Au (011). Its only failing is to predict that the 1×1 phase of Ir(011) is stable (by 0.01 J/m^2) over the 2×1 MR structure.

In conclusion, we have demonstrated for these fcc metals a good degree of transferability of the NRL-TB method to the surface environment. We have done this without including any surface data in the fitting scheme. We are currently examining other fcc and bcc metals in this regard as well as providing further tests of the method in the surface environment, such as examining the more complicated (111) and (001) reconstructions and surface stress trends.

ACKNOWLEDGMENTS

Funding for this work was provided by the Office of Naval Research. Codes developed under the CHSSI program of the DOD High Performance Computation Modernization Project have been utilized.

[1] J. C. Slater and G. F. Koster, Phys. Rev. **94**, 1498 (1954).
[2] R. E. Cohen, M. J. Mehl, and D. A. Papaconstantopoulos, Phys. Rev. B **50**, 14 694 (1994).
[3] M. J. Mehl and D. A. Papaconstantopoulos, Phys. Rev. B **54**, 4519 (1996).
[4] M. S. Daw and M. I. Baskes, Phys. Rev. Lett. **50**, 1285 (1983); Phys. Rev. B **29**, 6443 (1984).
[5] M. I. Baskes, Phys. Rev. Lett. **59**, 2666 (1987); M. I. Baskes, J. S. Nelson, and A. F. Wright, Phys. Rev. B **40**, 6085 (1989).
[6] J. Tersoff, Phys. Rev. Lett. **56**, 632 (1986); Phys. Rev. B **37**, 6991 (1988); Phys. Rev. B **38**, 9902 (1988).
[7] M. Z. Bazant, E. Kaxiras, and J. F. Justo, Phys. Rev. B **56**, 8542 (1997).
[8] D. A. Papaconstantopoulos and M. J. Mehl, J. Phys.: Condens. Matter **15**, R413 (2003).
[9] S. H. Yang, M. J. Mehl, D. A. Papaconstantopoulos, and M. B. Scott, J. Phys.: Condens. Matter **14**, 1895 (2002).
[10] N. Bernstein, M. J. Mehl, D. A. Papaconstantopoulos, N. I. Papanicolaou, M. Z. Bazant, and E. Kaxiras, Phys. Rev. B **62**, 4477 (2000).
[11] N. Bernstein, M. J. Mehl, and D. A. Papaconstantopoulos, Phys. Rev. B **66**, 075212 (2002).
[12] O. K. Andersen, Phys. Rev. B **12**, 3060 (1975); S.-H. Wei and H. Krakauer, Phys. Rev. Lett. **55**, 1200 (1985).
[13] F. Kirchhoff, M. J. Mehl, N. I. Papanicolaou, D. A. Papaconstantopoulos, and F. S. Khan, Phys. Rev. B **63**, 195101 (2001).
[14] M. I. Haftel, Phys. Rev. B **48**, 2611 (1993); M. I. Haftel, M. Rosen, T. Franklin, and M. Hettermann, Phys. Rev. Lett. **72**, 1858 (1994); M. I. Haftel and M. Rosen, Phys. Rev. B **51**, 4426 (1995).
[15] P. van Beurden and G. J. Kramer, Phys. Rev. B **63**, 165106 (2001).
[16] F. Raouafi, C. Barreteau, D. Spanjaard, and M. C. Desjonquères, Phys. Rev. B **66**, 045410 (2002).
[17] J. M. Khalifeh and T. M. Khajil, Surf. Sci. **469**, 118 (2000).
[18] A. Boussendel and A. Haroun, Thin Solid Films **325**, 201 (1998).
[19] G. Fabricius, A. M. Llois, M. Weissmann, and M. A. Khan, Phys. Rev. B **49**, 2121 (1994).
[20] C. F. Chen, Physica B **183**, 271 (1993).
[21] C. Barreteau, D. Spanjaard, and M. C. Desjonquères, Surf. Sci. **433–435**, 751 (1999).
[22] B. M'Passi-Mabiala, G. Moraitis, C. Demangeat, and A. Mikrani, Surf. Sci. **352–354**, 907 (1996).
[23] B. Piveteau, D. Spanjaard, and M. C. Desjonquères, Phys. Rev. B **46**, 7121 (1992).
[24] G. Moraitis, A. Mokrani, C. Demangeat, and B. M'passi-Mabiala, Surf. Sci. **364**, 396 (1996).
[25] B. Piveteau, D. Spanjaard, and M. C. Desjonquères, Phys. Rev. B **49**, 8402 (1994).
[26] J. S. Luo and B. Legrand, Phys. Rev. B **38**, 1728 (1988).
[27] M. Habar, L. Stauffer, H. Dreysse, and C. T. Wille, J. Phys.: Condens. Matter **12**, 7005 (2000).
[28] Y. Xie and J. A. Blackman, Phys. Rev. B **63**, 125105 (2001).
[29] Y. Xie and J. A. Blackman, Phys. Status Solidi A **189**, 763 (2002).
[30] C. Barreteau, R. Guirado-López, D. Spanjaard, M. C. Desjonquères, and A. M. Oles, Phys. Rev. B **61**, 7781 (2000).
[31] D. L. Adams, H. B. Nielsen, M. A. Van Hove, and A. Ignatiev, Surf. Sci. **104**, 47 (1981).
[32] W. Oed, H. Lidner, V. Starke, K. Heinz, K. Muller, and J. B Pendry, Surf. Sci. **224**, 179 (1989).
[33] D. L. Adams, L. E. Petersen, and C. S. Sorenson, J. Phys. C **18**, 1753 (1985).
[34] P. R. Watson, M. A. Van Hove, and K. Hermann, *Atlas of Surface Structures: Based on the NIST Surface Structure Database (SSD)* (American Chemical Society, Washington, DC, 1994), Vol. 1A.
[35] S. Hengrasmee, K. A. R. Mitchell, P. R. Watson, and S. J. White, Can. J. Phys. **58**, 200 (1980).
[36] W. Nichtl, N. Bickel, L. Hammer, K. Heinz, and K. Muller, Surf. Sci. **188**, L729 (1987).
[37] J. Quinn, Y. S. Li, D. Tian, H. Li, F. Jona, and P. M. Marcus, Phys. Rev. B **42**, 11 348 (1990).
[38] C. J. Barnes, M. Q. Ding, M. Lindroos, R. D. Diehl, and D. A. King, Surf. Sci. **162**, 59 (1985).
[39] W. Moritz and D. Wolf, Surf. Sci. **163**, L655 (1985).

[40] P. Fery, W. Moritz, and D. Wolf, Phys. Rev. B **38**, 7275 (1988).
[41] W. Hetterich, H. Niehaus, and W. Heiland, Surf. Sci. **264**, L177 (1992).
[42] P. Fenter and T. Gustafsson, Phys. Rev. B **38**, 10 197 (1988).
[43] J. W. M. Frenken, J. F. van der Veen, and G. Allan, Phys. Rev. Lett. **51**, 1876 (1983).
[44] E. Vlieg, K. Robinson, and K. Kern, Surf. Sci. **233**, 248 (1990).
[45] S. M. Foiles, M. I. Baskes, and M. S. Daw, Phys. Rev. B **33**, 7983 (1986).
[46] S. Foiles, Surf. Sci. **191**, L779 (1987).
[47] T. Ning, Q. Yu, and Y. Ye, Surf. Sci. **206**, L857 (1988).
[48] S. B. Sinnott, M. S. Stave, T. J. Raeker, and A. E. DePristo, Phys. Rev. B **44**, 8927 (1991).
[49] J. Wan, Y. L. Fan, D. W. Gong, S. G. Shen, and X. Q. Fan, Modell. Simul. Mater. Sci. Eng. **7**, 189 (1999).
[50] M. I. Baskes, Phys. Rev. B **46**, 2727 (1992).
[51] T. Yamaghishi, K. Takahashi, and T. Onzawa, Surf. Sci. **445**, 18 (2000).
[52] F. Mittendorfer, A. Eichler, and J. Hafneri, Surf. Sci. **423**, 1 (1999).
[53] M. Methfessel, D. Hennig, and M. Scheffler, Phys. Rev. B **46**, 4816 (1992).
[54] J. He and M. Scheffler, Phys. Rev. B **57**, 4768 (1998).
[55] A. Filippetti and V. Fiorentini, Surf. Sci. **377–379**, 112 (1997).
[56] G. Boisvert, L. J. Lewis, M. J. Puska, and R. M. Nieminen, Phys. Rev. B **52**, 9078 (1995).
[57] I. Galanakis, N. Papanikolaou, and P. H. Dederichs, Surf. Sci. **511**, 1 (2002).
[58] J. Jenkins, M. A. Petersen, and D. A. King, Surf. Sci. **494**, 159 (2001).
[59] P. J. Feibelman, Phys. Rev. B **51**, 17 867 (1995).
[60] K.-P. Bohnen and K. M. Ho, Electrochim. Acta **40**, 129 (1995).
[61] L. Vitos, A. V. Raban, H. L. Skriver, and J. Kollar, Surf. Sci. **411**, 186 (1998).
[62] M.-H. Tsai and K. C. Hass, Phys. Rev. B **52**, 16420 (1995).
[63] C. E. Bach, M. Giesen, H. Ibach, and T. L. Einstein, Phys. Rev. Lett. **78**, 4225 (1997).
[64] M. Elstner, D. Porezag, G. Jungnickel, J. Elsner, M. Haugk, T. Frauenheim, S. Suhai, and G. Seifert, Phys. Rev. B **58**, 7260 (1998).
[65] M. J. Mehl, D. A. Papaconstantopoulos, I. I. Mazin, N. C. Bacalis, and W. E. Pickett, J. Appl. Phys. **89**, 6880 (2001).
[66] A. J. Cox, J. G. Louderback, and L. A. Bloomfield, Phys. Rev. Lett. **71**, 923 (1993); A. J. Cox, J. G. Louderback, S. E Apsel, and L. A. Bloomfield, Phys. Rev. B **49**, 12 295 (1994).
[67] A. F. Voter and S. P. Chen, Mater. Res. Soc. Symp. Proc. 82, 175 (1987); R. J. Oh and R. A. Johnson, J. Mater. Res. **4**, 1195 (1989); J. Cai and Y. Y. Ye, Phys. Rev. B **54**, 8398 (1996).
[68] R. Pasianot, D. Farkas, and E. J. Savino, Phys. Rev. B **43**, 6952 (1991); **47**, 4149 (1993).
[69] L. D. Roelofs, S. M. Foiles, M. S. Daw, and M. I. Baskes, Surf. Sci. **234**, 63 (1990).
[70] M. J. Mehl and D. A. Papaconstantopoulos, *Topics in Computational Materials Science*, edited by C. Y. Fong (World Scientific, Singapore, 1998) Chap. 5.
[71] A. Gross, M. Scheffler, M. J. Mehl, and D. A. Papaconstantopoulos, Phys. Rev. Lett. **82**, 1209 (1999); C. H. Lekka, N. Bernstein, M. J. Mehl, and D. A. Papaconstantopoulos (to be published).
[72] J. Izquierdo, D. I. Bazhanov, A. Vega, V. S. Stepanyuk, and W. Hergert, Phys. Rev. B **63**, 140413 (2001); S. Pick, V. S. Stepanyuk, A. N. Baranov, W. Hergert, and P. Bruno, Phys. Rev. B **68**, 104410 (2003).
[73] W. R. Tyson and W. A. Miller, Surf. Sci. **62**, 267 (1977).
[74] F. Ercolessi, E. Tosatti, and M. Parrinello, Phys. Rev. Lett. **57**, 719 (1986).
[75] K. W. Jacobsen, J. K. Nørskov, and M. J. Puska, Phys. Rev. B **35**, 7423 (1987).
[76] J. Rudnick and E. A. Stern, Phys. Rev. B **7**, 5062 (1973); R. C. Kittler and L. M. Falicov, Phys. Rev. B **18**, 2506 (1978).
[77] R. H. Victora, L. M. Falicov, and S. Ishida, Phys. Rev. B **30**, 3896 (1984).
[78] J.-H. Cho and M. Scheffler, Phys. Rev. Lett. **78**, 1299 (1996).
[79] J. Xie and M. Scheffler, Phys. Rev. B **57**, 4768 (1998).
[80] R. P. Gupta, Phys. Rev. B **23**, 6265 (1981).
[81] A. P. Sutton, M. W. Finnis, D. G. Pettifor, and Y. Ohta, J. Phys. C **21**, 35 (1988).
[82] V. Fiorentini, M. Methfessel, and M. Scheffler, Phys. Rev. Lett. **71**, 1051 (1993).
[83] R. C. Cammarata, Surf. Sci. **279**, 341 (1992).
[84] R. J. Needs and M. Mansfield, J. Phys.: Condens. Matter **1**, 7555 (1989).